

Strong Motion Data of the 1994-2002 Earthquakes in Iran: A Catalogue of 100 Selected Records with Higher Qualities in the Low Frequencies

Mehdi Zare

Seismology Research Center, International Institute of Earthquake Engineering and Seismology (IIEES), Tehran, Iran, email: mzare@iiees.ac.ir

ABSTRACT: The recorded strong motion data in Iran since 1994 till the end of 2002 are investigated in order to investigate the well recorded (high signal to noise ratio) accelerometric data, specially in the long period ranges. The records having low signal to noise ratio in the frequency range of less than 0.3 Hz are excluded, and the rest of 100 records are processed and analyzed in this study. The site classification for these records is performed based on the receiver function method (estimating the H/V ratio for each of the recorded motions). According to this procedure, the number of the selected records were 46, 10, 16 and 28 for the site classes 1, 2, 3 and 4 respectively. The frequency contents of most of the records show dominant amplitudes between frequencies 0.2 and 10Hz. The Fmax values are systematically greater for the vertical components comparing to the horizontal ones. This selected catalog of 100 accelerograms obtained from 15 earthquakes provides a basis for the good quality/recent strong motion records in Iran, having good quality low frequencies contents. The response spectra of selected records having a PGA>0.05g are presented in the article and the normalized-mean spectra for the 4 site classes are introduced. The predominant periods of site classes 1, 2, 3 and 4 are found to be 0.09, 0.1, 0.13 and 0.2 sec for horizontal components and 0.08, 0.06, 0.11 and 0.15 sec for vertical components respectively.

Keywords: Strong motion; Data; Iran; Low frequency; Process; Record

1. Introduction

The Iranian strong motion data are investigated in order to find the earthquakes for which more than one accelerograms are recorded with higher qualities in lower frequencies. In this study, the attention is paid to better quality records and those that could have less low frequency noises.

The accelerometric network of Iran comprises of more than 1500 stations, for which more than 3500 records are already recorded by March 2003. The records obtained from the great events are now available on web site of BHRC (Building and Housing Research Center; the organization who maintains the Iranian national strong motion network). The data studied for the Changureh 2002 earthquake in this paper are taken from the BHRC web site [8]. The

stations are selected in all over the country, however, according to the importance of the capital, more than 30 stations are installed around Tehran (to be expanded to a local network of more than 50 stations). Meanwhile, according to higher seismicity of Zagros belt, and higher population density in this region (southwest and western Iran) comparing to eastern and southeastern Iran, more stations are selected in Zagros. Therefore, most of the records are actually corresponding to the Zagros belt.

The National Iranian Strong Motion network is installed first with the Kinematics SMA-1 analog instruments installed since 1975, and then they have been gradually expanded by the SSA-2 digital instruments since the Manjil earthquake of 1990;

16, 18, 19], along with the details on the selected records. The coordinates of the epicenters and the strong motion stations are given as well in Table (1). These stations are shown in Figures (2a) to (2d) based on their site conditions; of class '1' to class '4', respectively. These site classes are assigned based on a detailed site effect study in Iran on the strong motion station [20].

This database is composed by fairly well known source parameters which were very well recorded, and for which no source data was directly available. The moment magnitude and hypocentral distance for these records have thus been estimated directly from the strong motion records. The hypocentral distance was obtained from the $S-P$ time difference, while the seismic moment was directly calculated from the level of acceleration spectra plateau and the corner frequency [2].

The magnitude range for the whole dataset of

records was 4.6-7.2, see Table (2). The distributions of magnitude against hypocentral distance are shown in Figures (3) and (4a) to (4d) for different site classes. The range for hypocentral distance is 12-167 km. The focal depth range for the events relocated recently by Maggi et al [15] is 5-14 km (column 21 of Table (1)), and the teleseismic information on focal depths are excluded from Table (1), since such type of determination is very imprecise [2]. The two horizontal components of each record are included separately in the study, therefore the number of the horizontal records entered to the regressions was twice the vertical ones.

2.1. Filtering of the Accelerograms

In this study, the signal to noise ratio was considered to be significant only when the signal to noise ratio R_{sn} for both components exceeds a given threshold value, taken equal to 3. The signal to noise

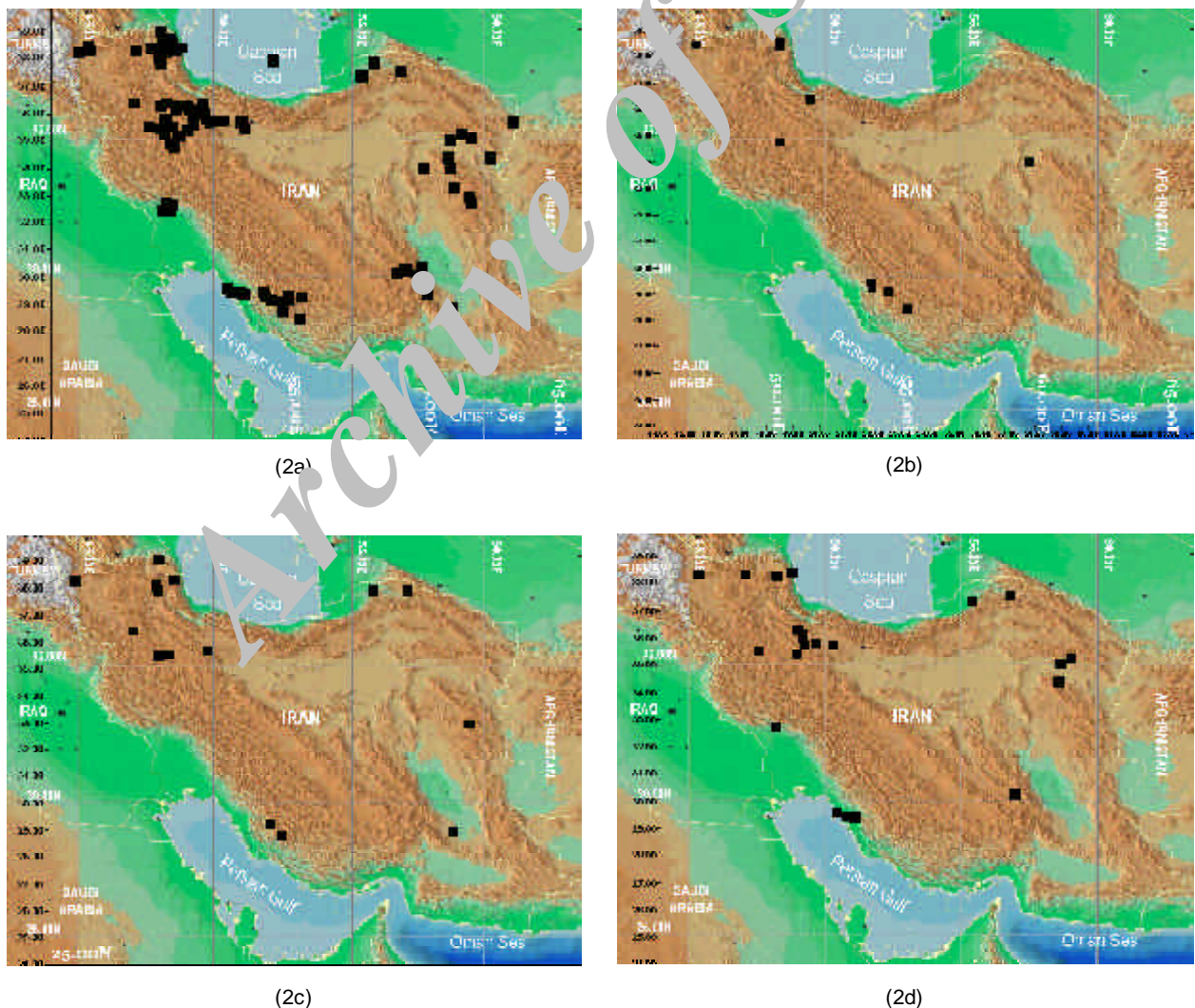


Figure 2. The locations of the stations in which the records are selected, distinguished based on the site classes; 2a: class '1'; 2b: class '2'; 2c: class '3'; 2d: class '4'. The base maps are taken from USGS Digital Data Series (2001).

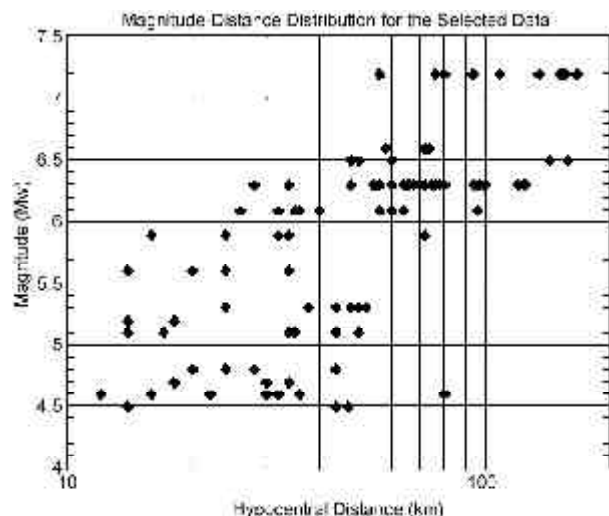
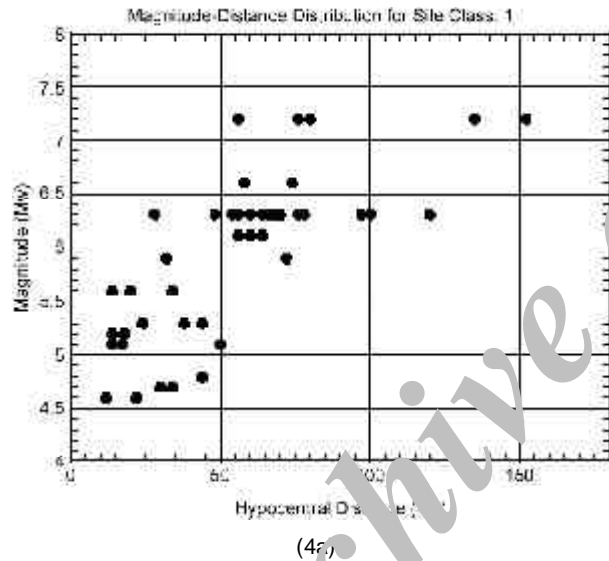


Figure 3. The magnitude-distribution for all of the data presented in Table (1).

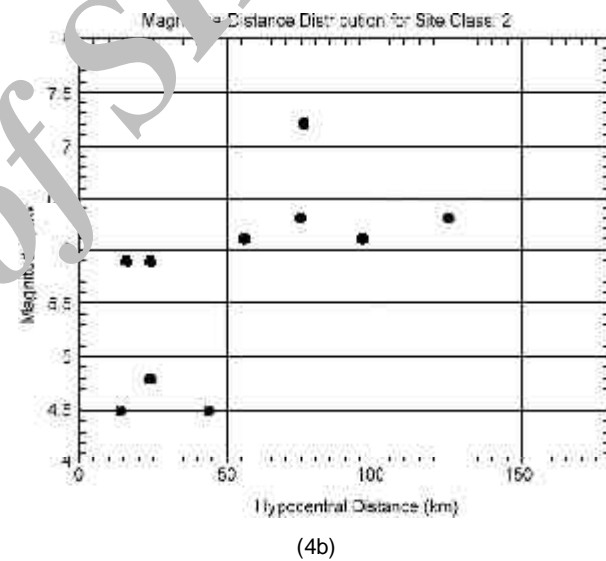
ratio (R_{sn}) is computed (as estimated by Theodoulidis and Bard [2]) as:

$$R_{sn} = \frac{S(f)}{\sqrt{t_1}} / \frac{N(f)}{\sqrt{t_2}} \quad (1)$$

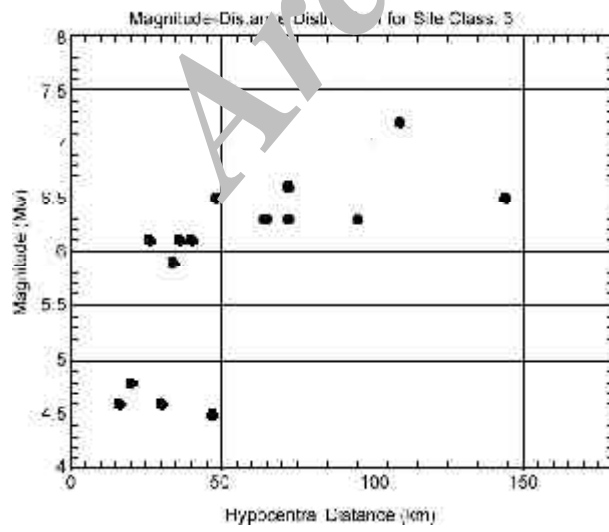
Where t_1 and t_2 are the window duration for the signal and noise parts, respectively. Since the records applied in this study are all digitally recorded, the time windows for noise parts (t_2) are selected before the p-onset (in the pre-event part of the records, mostly from 0 to 4 seconds, in the selected records). A R_{sn} ratio over 3 is selected as the proper ratio to distinguish the signal from the noise. The data having low signal qualities below 0.3Hz are excluded in order to keep the records having acceptable low frequency contents.



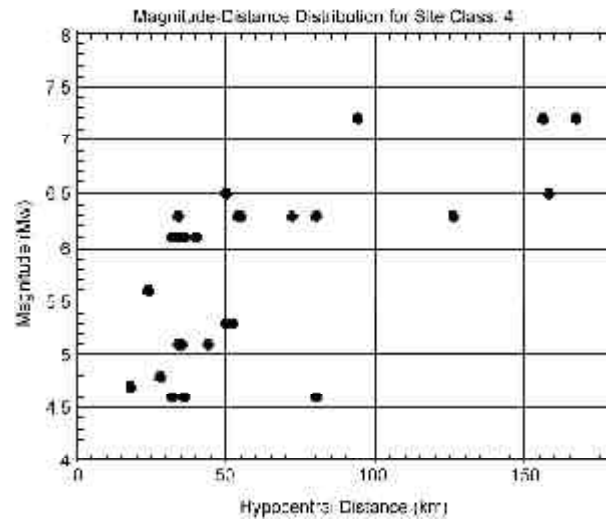
(4a)



(4b)



(4c)



(4d)

Figure 4. The magnitude-distance distribution for stations on different site classes; Figure (4a): class '1'; Figure (4b): class '2'; Figure (4c): class '3'; Figure (4d): class '4'.

The result of the estimation of R_{sn} ratios for four greater records (after processing, having a peak ground accelerations greater than 300cm/sec^2) obtained in the

stations of Zarrat, Zanjiran, Karigh and Avaj (Table (1)) are shown in Figures (5) to (8), respectively. The high-pass and low pass filters are hence selected for

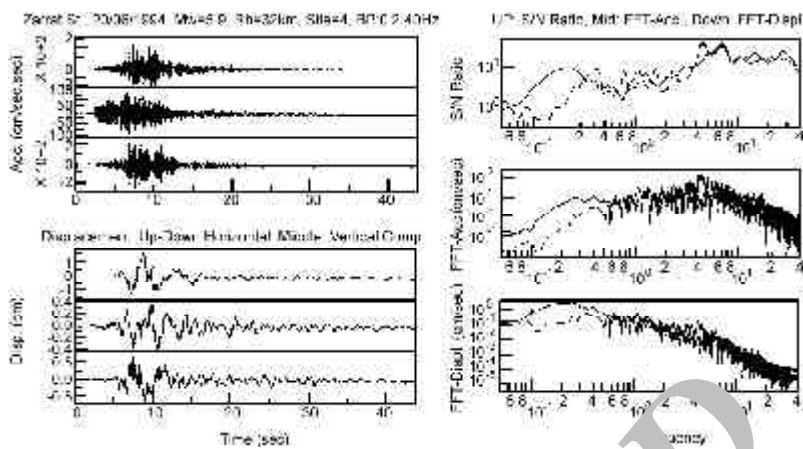


Figure 5. The processing of the Zarrat record of 20/06/1994, Mw 5.9 earthquake; above-left: three-component accelerograms (up and down traces are the horizontal components and the middle trace is the vertical one), below-left: double integrated displacement time-histories, above-right: Signal to noise ratio, middle-right: FFT of Accelerations, below-right: FFT of displacements. The dashed lines indicate the vertical components and the continuous lines are for horizontal ones.

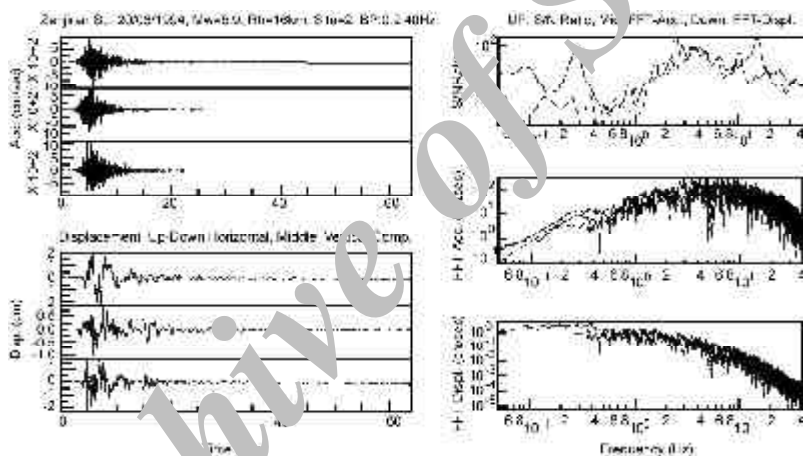


Figure 6. The processing of the Zanjiran record of 20/06/1994, Mw 5.9 earthquake; above-left: three-component accelerograms (up and down traces are the horizontal components and the middle trace is the vertical one), below-left: double integrated displacement time-histories, above-right: Signal to noise ratio, middle-right: FFT of Accelerations, below-right: FFT of displacements. The dashed lines indicate the vertical components and the continuous lines are for horizontal ones.

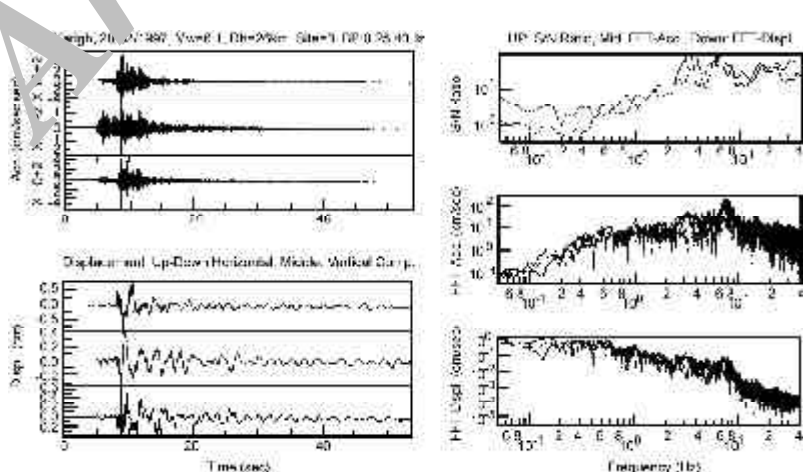


Figure 7. The processing of the Karigh record of 28/02/1997, Mw 5.9 earthquake; above-left: three-component accelerograms (up and down traces are the horizontal components and the middle trace is the vertical one), below-left: double integrated displacement time-histories, above-right: Signal to noise ratio, middle-right: FFT of Accelerations, below-right: FFT of displacements. The dashed lines indicate the vertical components and the continuous lines are for horizontal ones.

the parts having the signal to noise ratio greater than 3, and are given in the column 7 of Table (1) (same filter bands are found for both horizontal and vertical

components).

The signal to noise ratios for all records are given in Figures (9) and (10) for horizontal and vertical

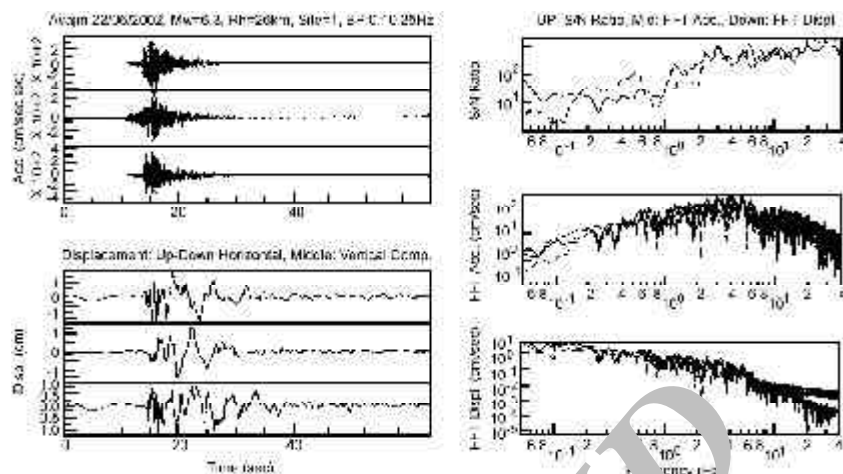


Figure 8. The processing of the Avaj record of 22/06/2002, Mw 6.3 earthquake; above-left: three-component accelerograms (up and down traces are the horizontal components and the middle trace is the vertical one), below-left: double integrated displacement time-histories, above-right: Signal to noise ratio, middle-right: FFT of Accelerations, below-right: FFT of displacements. The dashed lines indicate the vertical components and the continuous lines are for horizontal ones.

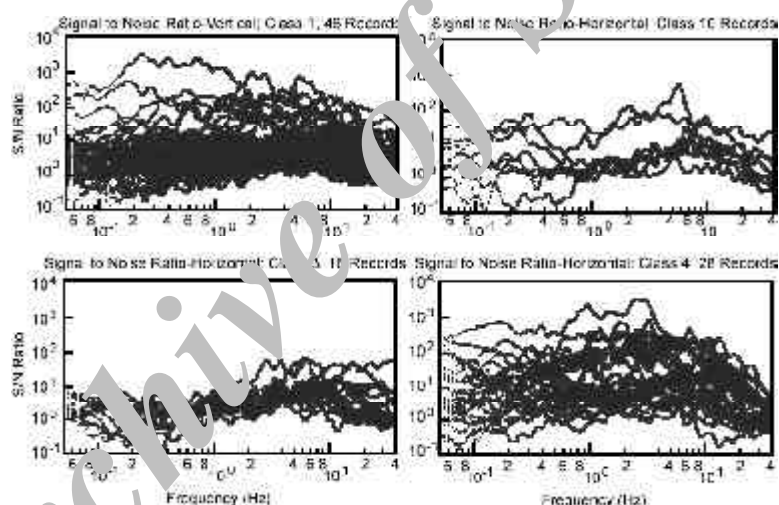


Figure 9. The signal to noise ratios for all of the records, distinguished for site classes '1' (above-left), '2' (above-right), '3' (below-left), and '4' (below-right); horizontal components.

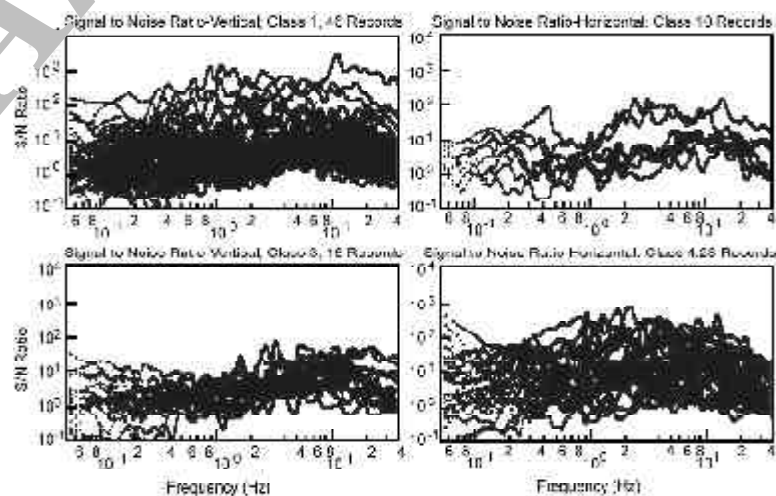


Figure 10. The signal to noise ratios for all of the records, distinguished for site classes '1' (above-left), '2' (above-right), '3' (below-left), and '4' (below-right); vertical components.

components respectively. These figures show the dominance of the frequency band of the good quality signals between 0.2 and 10Hz for most of the cases. However the qualities of the signals are found to be lower for records assigned to site class '3', comparing to other site classes.

2.2. Magnitude Values

Magnitude used here is the moment magnitude, to give a uniform and reliable scale for comparison of different parameters. The moment magnitude was systematically calculated for all selected records, which are well recorded earthquakes (with little noise).

The source model used to estimate the moment magnitude in this study is based on Haskell [13], who proposed a simple source model for the estimation of high frequency ground motions. The simple seismic source models are explained by Aki [1] and Brune [6, 7]. In this model, the far field displacement spectrum is characterized by a flat level \bar{W}_0 proportional to M_o at long periods, a corner frequency f_c proportional to inverse of the source dimension, and a high frequency spectral decay in the form $(f/f_c)^g$. Taking the g values as 2 or 3, we have the ω -square or ω -cube model, respectively (ω is the angular frequency in radians per second, equal to $2\pi f$). Hanks [10] has shown that with a ω -square model, for which the acceleration spectra will be flat after the corner frequency, f_c , the high frequency decay may be explained by the attenuation caused by the path effects. The more complicated ω -cube model [7], as a dynamic model, shows that the rupture nucleation generates high frequency energy, which is proportional to ω^3 . As proposed by Hanks and Kanamori [11], the displacement spectra may be represented by;

$$\bar{W} = \frac{\bar{W}_0}{1 + \left(\frac{f}{f_c}\right)^\gamma} \quad (2)$$

If \bar{W}_0 is the value of the flat part of the displacement spectrum, the value of the flat part of the acceleration spectrum, A_o , may be related to $\bar{W}(0)$ with $A_0 = \bar{W}_0 \cdot \omega_c^2$ proportional to the seismic moment; M_o . For far-field S-waves, due to a double couple source embedded in an elastic, homogeneous, isotropic bounded medium [11], we have:

$$M_o = \frac{A_0}{(2\pi f_c)^2} \cdot \frac{4\pi R_h \cdot \rho \cdot \beta^3}{R'_{\theta\phi} \cdot F_s} \quad (3)$$

Where β is the shear wave velocity of the medium; ρ is the density of elastic medium; around $(2.8 \times 10^3) \text{ kg/m}^3$, R_h is the hypocentral distance, $R'_{\theta\phi}$ is the double couple radiation pattern for SH or SV waves (about 0.6 in average), F_s is the free space amplification factor (to be taken equal to 2) [3]. In the following, to calculate M_o (in N-m), we take b equal to 3500 m/sec [14]; $\rho = 2.8 \times 10^3 \text{ kg/m}^3$.

Hanks and Kanamori [11] defined a new magnitude scale based on the seismic moment, that is more reliable measure of the size of the great earthquakes. This scale with taking into account the coefficients for N-m unit of M_o , could be written as follows:

$$M_w = 0.667 M_o - 6.0 \quad (4)$$

The author has used the formula (3) and (4) to calculate M_w for the events listed in Table (1).

Based on the estimated M_w for each of the earthquakes, and after filtering the records (explained in 2.1) the values of peak ground acceleration (PGA) for different components are shown in columns 8 to 10 of Table (1). The estimated corner frequencies (f_c) and maximum frequencies (f_{max}) for horizontal and vertical components are given in columns 11 to 13 of Table (1). The distribution of PGA against magnitudes and hypocentral distances are shown in Figure (11). The horizontal and vertical PGA are shown against the horizontal and vertical f_{max} , respectively, in Figure (12). The corner frequencies are compared as well with the PGA in Figure (13), and with f_{max} values in Figure (14). These figures show that most of the data are distributed over the hypocentral distances of 10 to 100 kilometers and the f_{max} values found for the vertical components are systematically greater for vertical components.

2.3. Site Classification

The site classes are estimated based on the transfer function method, in which the H/V amplification function is calculated, in order to find the fundamental frequency of the site [21]. However the site specific studies are performed for some of the sites studied in this paper (Zarrat, Firouzabad, Zanjiran, Hosseiniyeh, Saadabad, Shabankareh, Dasht-Bayaz, Gonabad, Kerman, Buin-Zahra, Abhar and Eshtehard; Table (1)) in view point of the microtremor measurements and the seismic wave velocity profiling [21]. The formulation used for the H/V method is based on the spectral ratio (R_{hv}) between the smoothed horizontal components and the smoothed vertical component:

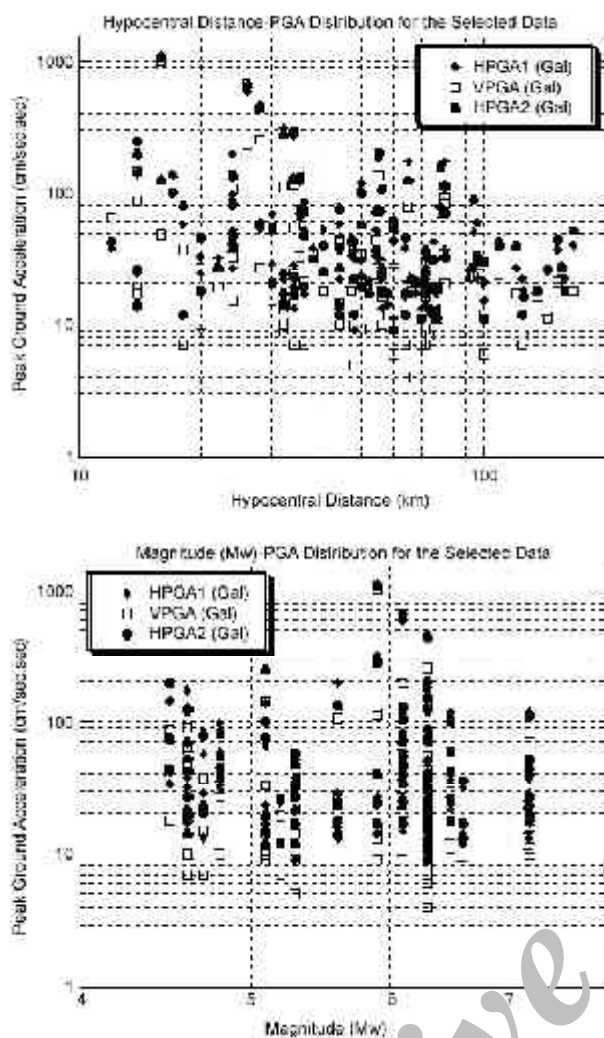


Figure 11. The distribution of the records against hypocentral distance (above) and magnitude (below).

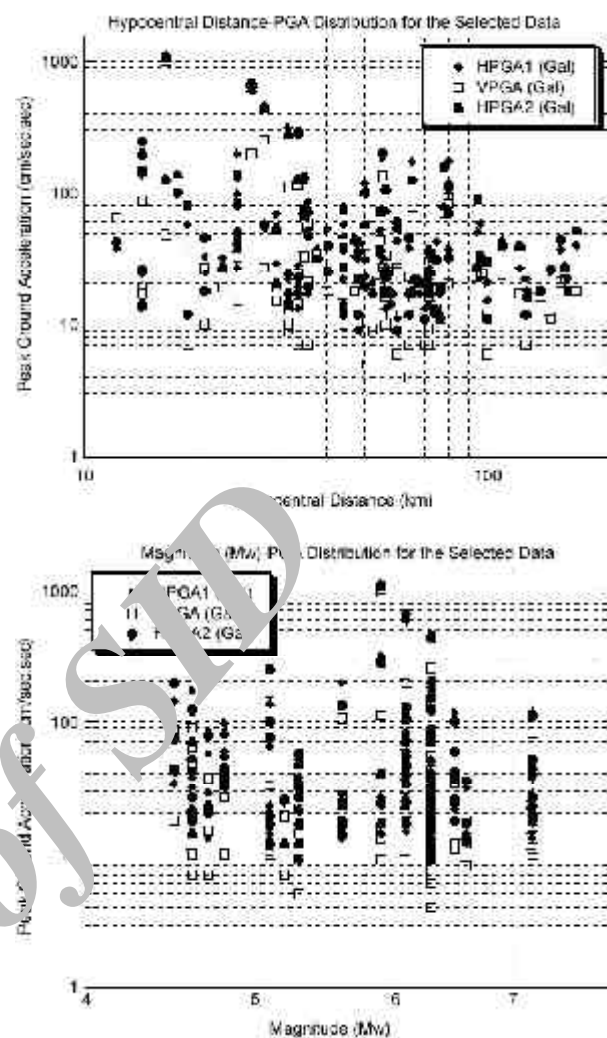


Figure 12. The distribution of Fmax values against PGA for horizontal components (above) and vertical components (below).

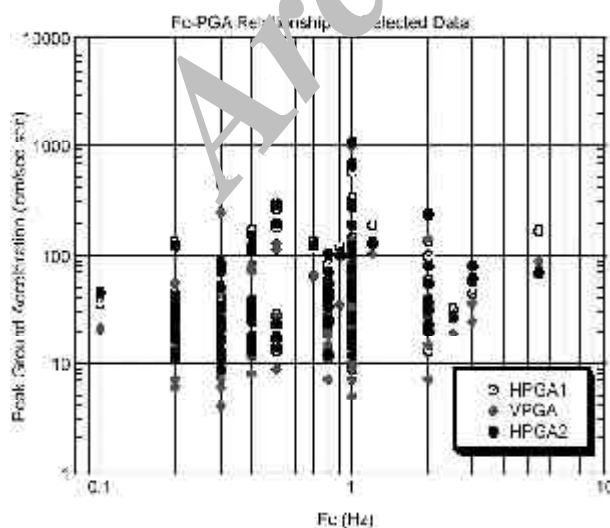


Figure 13. The distribution of fc values against PGA for horizontal and vertical components.

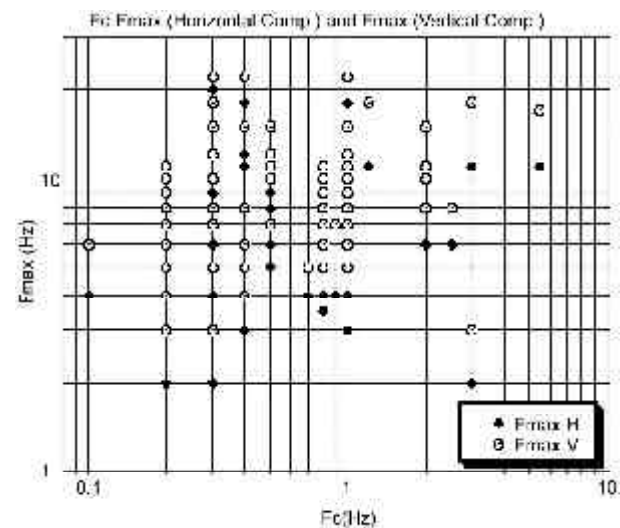


Figure 14. The distribution of fc values against fmax for horizontal and vertical components.

$$R_{hv} = \frac{\sqrt{\frac{S_{H1}^2}{2\sqrt{T_{H1}}} + \frac{S_{H2}^2}{2\sqrt{T_{H2}}}}}{\frac{S_v(f)}{\sqrt{T_v}}} \quad (5)$$

Where T_{H1} , T_{H2} and T_V are the signal duration for the horizontals and vertical components respectively. Since the same time windows are used the same for all components, this relationship might be simplified as;

$$R_{hv} = \frac{\sqrt{S_{H1}(f) + S_{H2}(f)}}{S_v(f)} \quad (6)$$

Site class '1' is defined as sites that do not exhibit any significant amplification below 15Hz. It corresponds to rock and stiff sediment sites with an average S-wave velocity over the top 30 meters in excess of 700m/sec. Site class 2 determined as sites for which the receiver function (RF) exhibits a fundamental peak exceeding 3 at a frequency located between 5 and 15Hz. It was shown to correspond to stiff sediments and/or soft rocks with V_{s30} between 500 and 700 m/sec. Site class 3 is representative for the sites for which RF shows the peaks between 2 and 5Hz and corresponds to the alluvial sites with V_{s30} between 300 and 500m/sec. Finally site class 4 is defined as sites for which RF indicates the peaks in frequencies below 2Hz, and it may be viewed as corresponding to thick soft alluvium. This ranking was the result of the geotechnical measurements on 50 sites (compressional and shear wave velocity

and microtremors) and the calculation of the receiver function for the strong motions using the three component accelerograms. This categorization show some similarity to that of Boore et al [4, 5] (based on the average V_s for the 1st 30m) for the northwestern American data. The average V_s limits to distinguish the site classes in Boore et al [4, 5] reports are 180m/sec, 360m/sec, 750m/sec and greater than 750m/sec (to be compared with our values of 300, 500 and 700m/sec).

The H/V amplification ratios are shown for all records in Figure (15). These spectral ratios are averaged in Figure (16) for each of the four site classes. These two figures coincide well the defined criteria by Zaré et al [21] in order to classify the sites of the strong motion stations based on the frequency band or the predominant frequency of the site as described above.

2.4. Distance Variables

When discussing the choice of the "distance parameter" one must keep in mind the significant uncertainties in seismic epicenter localization and large uncertainties in determining of focal depths for the Iranian earthquakes. It is important however to define this parameter so that the future application of these data to establish the attenuation laws will be easy.

We have decided to define the distance variable for the regression as the "hypocentral distance". This distance is controlled by the difference in the arrivals of the compressional and shear wave for each record. Such information is available without any ambiguity

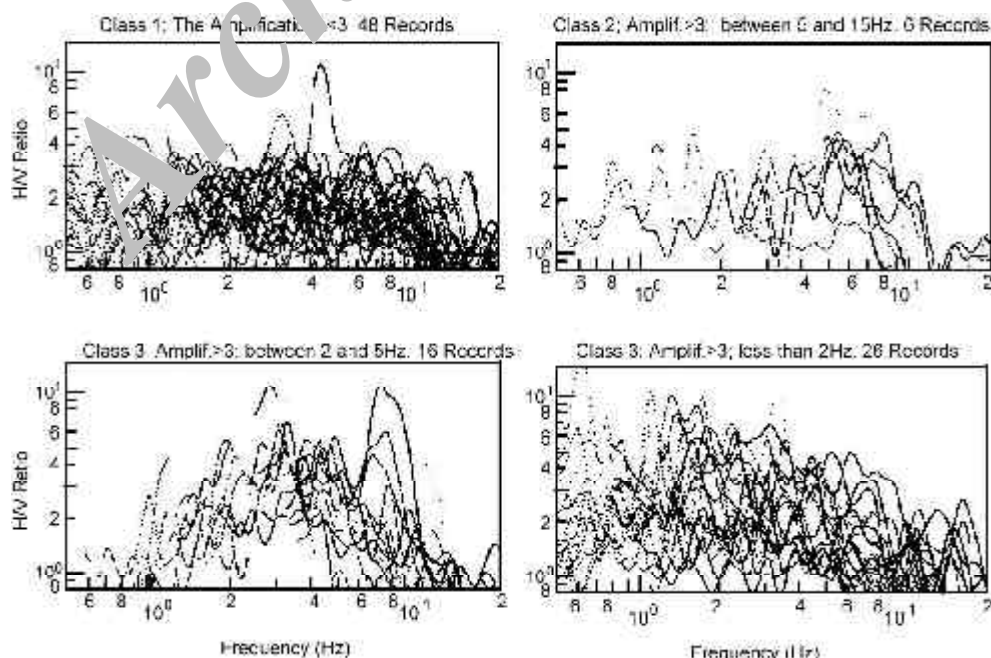


Figure 15. The H/V ratios distinguished for site classes '1' (above-left), '2' (above-right), '3' (below-left), and '4' (below-right).

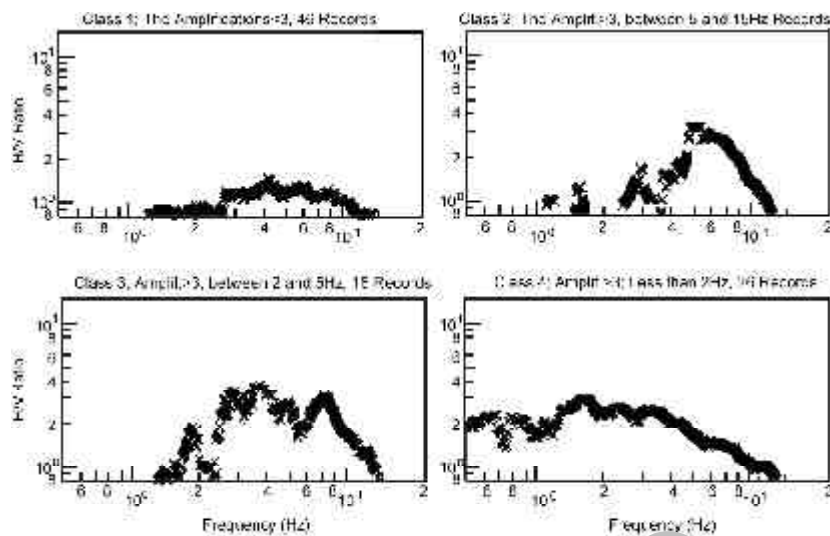


Figure 16. The average of H/V ratios distinguished for site classes '1' (above-left), '2' (above-right), '3' (below-left), and '4' (below-right).

only with the SSA-2 digital records (all records studied herein were obtained by such type of recorders). The results of these estimations are given in column 23 of Table (1).

2.5. Fault mechanism

According to the regional tectonic conditions of the Iranian plateau, the fault mechanisms of most of the earthquakes are compressional, strike-slip or a combination of these two mechanisms. The fault mechanisms of most of the earthquakes used in the present study were strike-slip, compressional or a combination of these two mechanisms (Harvard Seismology web site, 2003 [15], PEIC web site, 2003 [16]). The available information on focal mechanisms are presented in column 22 of Table (1). In an earlier study [2, 20], it is shown that the focal mechanisms of the records for which the source parameters could be found comprise mostly strike-slip/reverse mechanism, pure strike slip, pure reverse and pure vertical plane.

3. Response Spectra

The response spectra of the studied records are studied. The spectra for the greater events (records having a greatest $PGA \geq 0.05g$, in one or all of the three components) are selected for comparison in this paper. The records that had such condition for the site classes 1, 2, 3 and 4 have been 9, 6, 8, and 16 respectively (Table (1)). Having two horizontal components, the horizontal response spectra applied in the comparisons are doubled the mention numbers. The response spectra for the site class '1'

are shown in Figure (17) ('a' and 'b' for horizontal and vertical components, respectively). The spectra

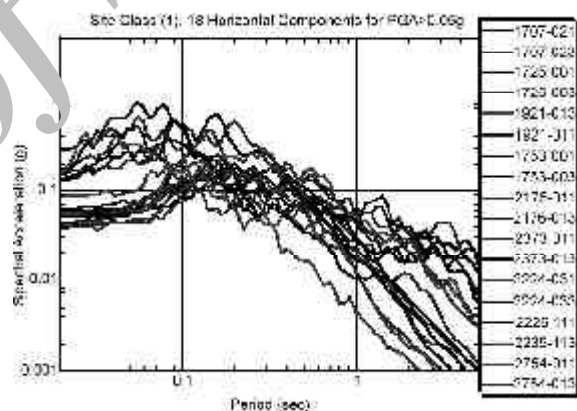


Figure 17a. The response spectra for 11 records obtained on the site class '1' (22 horizontal components).

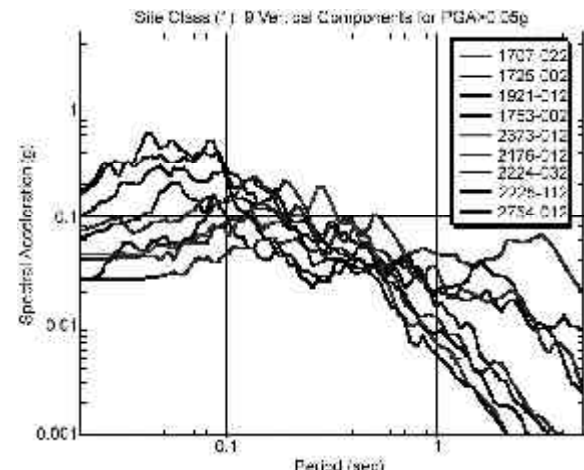


Figure 17b. The response spectra for 11 records obtained on the site class '1' (vertical components).

for the site classes '2', '3' and '4' are shown in Figures (18), (19) and (20), respectively. The values of the normalized spectra for the site classes 1 to 4 are presented in Figures (21), (22), (23) and (24) respectively. The normalized response spectra are

compare for 4 site classes in Figures (25a) and (25b), for horizontal and vertical components, respectively. According to these figures, the response spectra for different site classes are distinguished. As it is clear in Figures (21) to (24), the softer the site, the longer

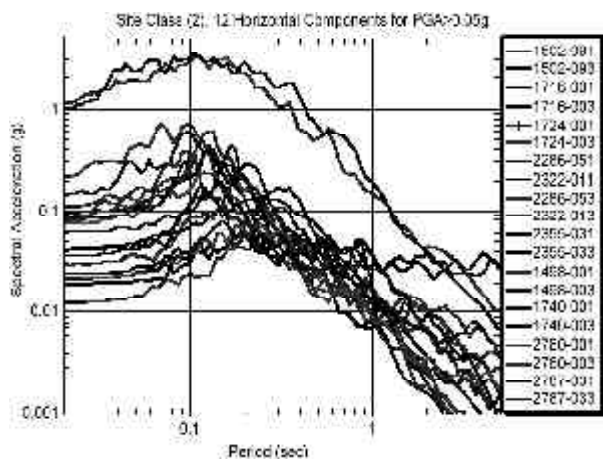


Figure 18a. The response spectra for 6 records obtained on the site class '2' (12 horizontal components).

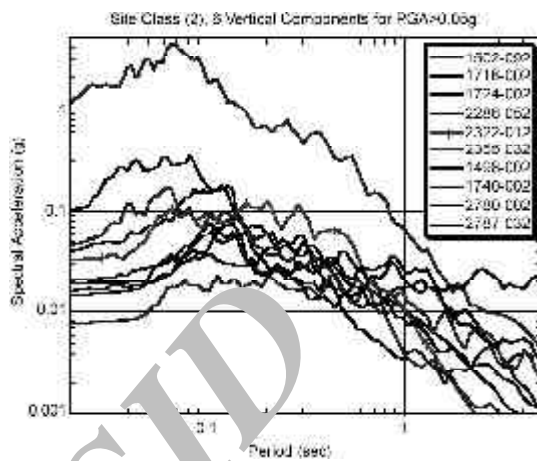


Figure 18b. The response spectra for 6 records obtained on the site class '2' (vertical components).

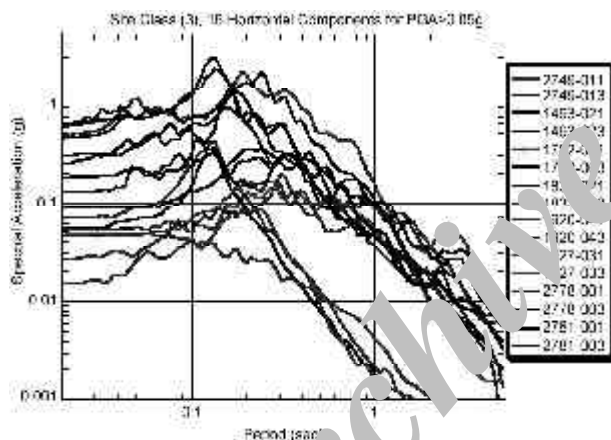


Figure 19a. The response spectra for 8 records obtained on the site class '3' (16 horizontal components).

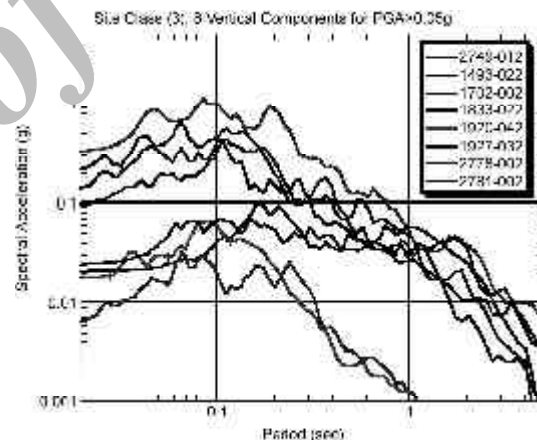


Figure 19b. The response spectra for 8 records obtained on the site class '3' (vertical components).

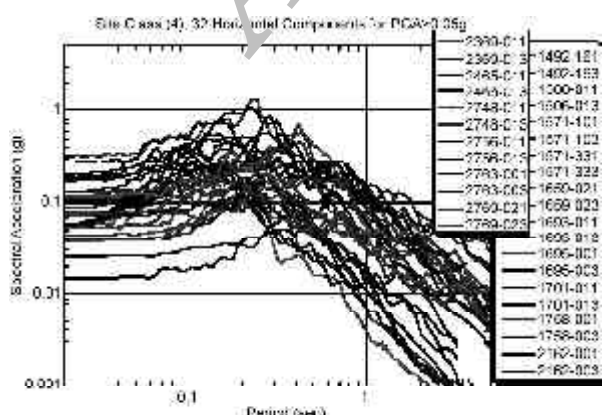


Figure 20a. The response spectra for 16 records obtained on the site class '4' (32 horizontal components).

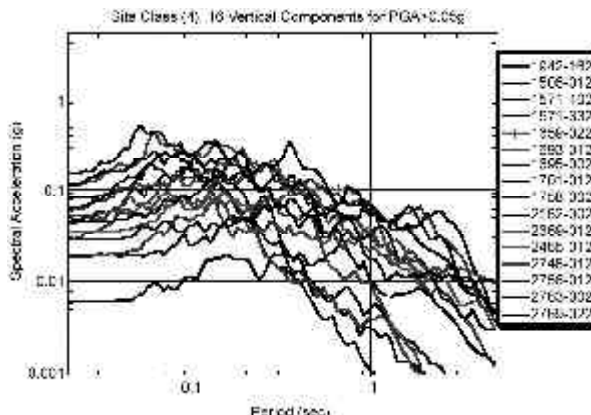


Figure 20b. The response spectra for 16 records obtained on the site class '4' (vertical components).

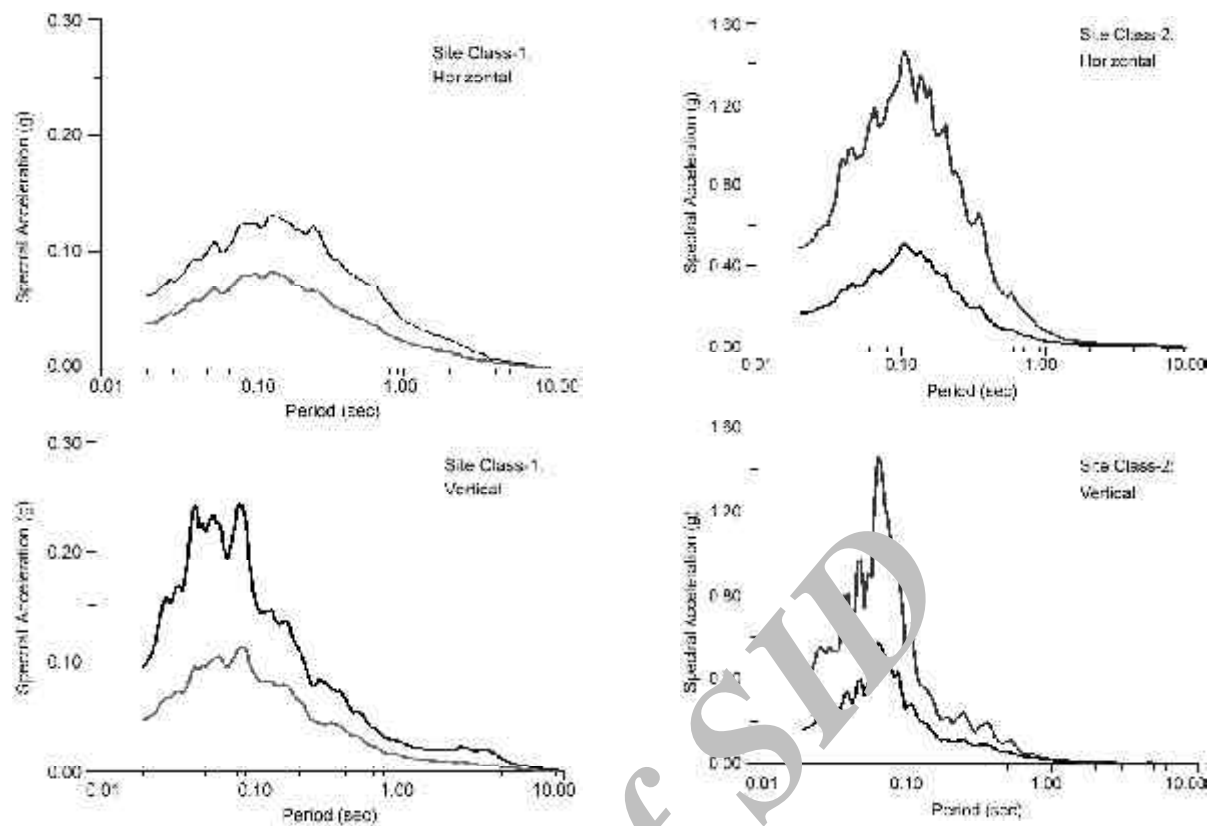


Figure 21. The mean and mean plus sigma response spectra for site class "1" (Horizontal; up, and vertical; down).

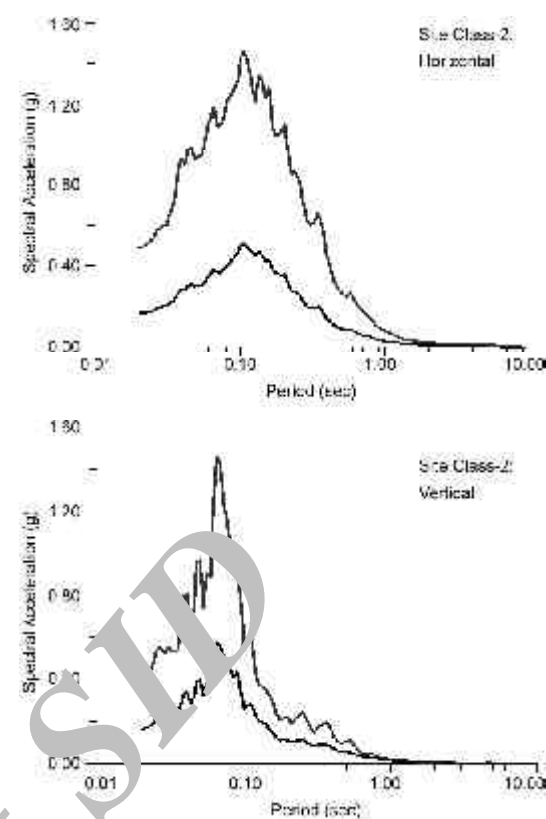


Figure 22. The mean and mean plus sigma response spectra for site class "2" (Horizontal; up, and vertical; down).

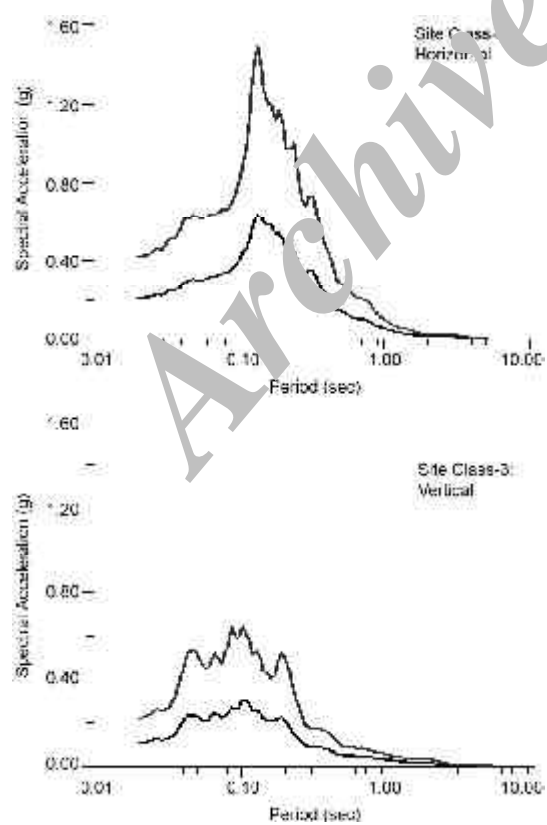


Figure 23. The mean and mean plus sigma response spectra for site class "3" (Horizontal; up, and vertical; down).

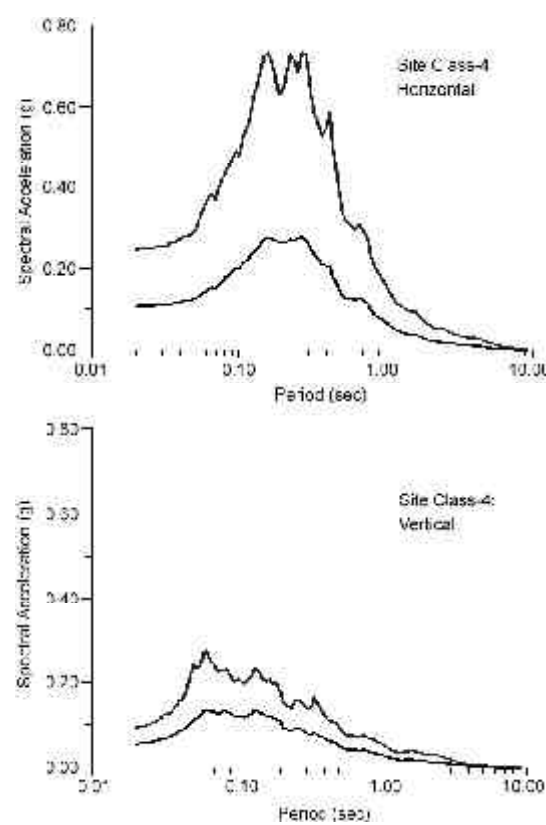


Figure 24. The mean and mean plus sigma response spectra for site class "4" (Horizontal; up, and vertical; down).

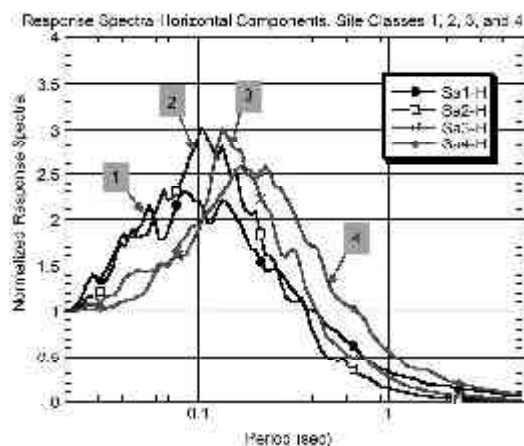


Figure 25a. The normalized response spectra for site classes '1, 2, 3, and 4' for horizontal component.

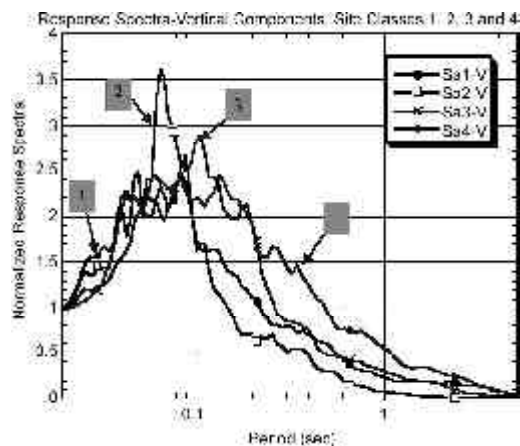


Figure 25b. The normalized response spectra for site classes '1, 2, 3, and 4' for vertical component.

the predominant period of response spectra will be. The predominant periods of 0.09, 0.1, 0.13 and 0.2 seconds are found on the horizontal components, for the site classes 1, 2, 3 and 4, respectively. These values on the vertical components are 0.08, 0.06, 0.11 and 0.15 seconds for the site classes 1, 2, 3 and 4, respectively. This shows the difference between frequency contents of the horizontal and vertical components.

4. Discussions

The selected records are listed in Table (1). The records are presented based on their codes assigned by the Building and Housing Research Center, BHRC [8]), station name, site class, band-pass filter selected for each record, *PGA* (the greater of three components), the event's date, coordinates, epicentral region, reported magnitude, focal depths, focal mechanisms and the hypocentral distances. The hypocentral distances are estimated for each record based on the s-p arrival time method. The displacement time-histories (after 2 times integrals), as well as the *FFT*'s of displacement are shown as well, for 4 greater records in order to indicate the relative stability of the mentioned records in low frequencies. 100 records corresponding to 15 earthquakes are finally selected.

The selected records have different frequency contents and specifications. This difference corresponds to the magnitude and hypocentral distances, as well as to the instrument type. Most of the records are noisy in the frequencies less than 0.3Hz. However, some records show high signal to noise ratios in the frequency band of 0.3Hz or lower. These records are listed in Table (1).

The response spectra for horizontal and vertical components are classified as well. The class '4' shows that the form of the response spectra is shifted towards the longer periods. The normalized spectra show that the predominant periods change in different site classes between 0.09 and 0.2 seconds for horizontal components. The normalized vertical spectra for the class '1' shows lower the predominant period than that of class '1'. This may be resulted from the number of the available records selected for these classes (6 records for site class '2'). Otherwise such problems should be controlled in the further studies based on the recently obtained digital records (after 2000). Except for the Changureh (22 June 2002) earthquake, such better quality recent records were not available at the time of the present study.

5. Conclusion

This study was aimed to select the recent strong motion records obtained in Iran (1994-2002) in order to study the earthquakes for which several records (2 or more) are available. 100 records relating to 15 earthquakes are selected. These records had better quality in the frequency bands less than 0.3Hz. These data seem to provide a sufficient basis for the long period strong motion studies, such as rupture modeling and strong motion displacement studies. The normalized response spectra for the records having greater *PGA* values shows the longer predominant periods for the softer site classes.

References

1. Aki, K. (1967). "Scaling Law of Seismic Spectrum", *J. Geoph. Res.*, **72**, 1217-1231.

2. Bard P.-Y., Zaré, M., and Ghafory-Ashtiany, M. (1998). "The Iranian Accelerometric Data Bank, A Revision and Data Correction", *Journal of Seismology and Earthquake Engineering*, **1**(1), 1-22.
3. Boore, D.M. (1986). "Short-Period P and S Wave Radiation from Large Earthquakes: Implications for Spectral Scaling Relations", *Bull. Seismol. Soc. of America*, **76**(1), 43-64.
4. Boore, D.M., Joyner, W.B., and Fumal, T.E. (1993). "Estimation of Response Spectra and Peak Accelerations from Western North American Earthquakes: An Interim Report", U.S. Geol. Survey, Open-File Report: 93-509, 72 p.
5. Boore, D.M., Joyner, W.B., and Fumal, T.E. (1993). "Estimation of Response Spectra and Peak Accelerations from Western North American Earthquakes: An Interim Report", U.S. Geol. Survey, Open-File Report: 94-127, 40 p.
6. Brune, J.N. (1970). "Tectonic Stresses and the Spectra of Seismic Shear Waves", *J. Geoph. Res.*, **75**, 4997-5009.
7. Brune, J.N. (1971). "Corrections", *J. Geoph. Res.*, **76**, 5002 p.
8. Building and Housing Research Center (BHRC) Web Site (2003). <http://www.bhrc.gov.ir/>.
9. Earthquake Research Institute (ERI, University of Tokyo), Web Site (2002). http://www.eic.eri.u-tokyo.ac.jp/EIC/EIC_News/020622.gif.
10. Hanks, T.C. (1982). "b Value and ω^g seismic Source Models: Implications for Tectonic Stress Variations Along Active Crustal Fault Zones", *J. Geoph. Res.*, (84), 2235-2242.
11. Hanks, T.C. and Kanamori, H. (1979). "A Moment Magnitude Scale", *J. of Geoph. Res.*, **84**(B5), 2348-2350.
12. Harvard University, Seismology Department, Web Site(2003).<http://www.seismology.harvard.edu/>.
13. Haskell, N.A. (1964). "Total Energy and Energy Spectral Density of Elastic Wave Radiation from Propagating Faults", *Bull. Seism. Soc. of America*, **54**, 1811-1841.
14. Kennet, B.L.N. and Engdahl, E.L. (1991). "Travel Times for Global Earthquake Location and Phase Identification", *Geoph. J. Int.*, **105**, 429-456.
15. Maggi, A., Priestley, K., and Jackson, J. (2003). "Focal Depths of Moderate and Large Size Earthquakes in Iran", *Journal of Seismology and Earthquake Engineering (JSEE)*, **4**(2-3), 1-10.
16. National Earthquake Information Center, USGS (2003). Web Site, <http://wwwneic.cr.usgs.gov/>.
17. Panza, G.F., Romanelli, F., and Vaccari, F. (2001). "Seismic Wave Propagation in Laterally Heterogeneous Anelastic Media: Theory and Application in Seismic Zonation", *Advances in Geophysics*, **43**, 1-95.
18. Theodoulidis, N. and Bard, P.-Y. (1995). "(H/V) Spectral Ratio and Geological Condition; An Analysis of Strong Motion Data from Greece and Taiwan, (SMART-1)", *Soil Dynamics and Earthquake Engineering*, **14**, 177-197.
19. United States Geological Survey (USGS), (2001). Digital Data Series DDS-62-C.
20. Zaré, M. (1999). "Contribution à L'étude Des Mouvements Forts en Iran: Du Catalogue Aux Lois D'atténuation", Université Joseph Fourier, Thèse de Doctorat (Ph.D. Thesis), 237 p.
21. Zaré, M., Bard, P.-Y., and Ghafory-Ashtiany, M. (1999). "Site Characterizations for the Iranian Strong Motion Network", *J. of Soil Dynamics and Earthquake Engineering*, **18**(2), 101-121.